LAWRENCE
LIVERMORE
NATIONAL
LABORATORY

LLNL-CONF-472011

Impact of Spherical Inclusion Mean Chord Length and Radius Distribution on Three-Dimensional Binary Stochastic Medium Particle Transport

P. S. Brantley, J. N. Martos

March 4, 2011

International Conference on Mathematics and Computational Methods Applied to Nuclear Science and Engineering
Rio de Janeiro, Brazil
May 8, 2011 through May 12, 2011

Disclaimer

International Conference on Mathematics and Computational Methods Applied to Nuclear Science and Engineering (M&C 2011)
Rio de Janeiro, RJ, Brazil, May 8-12, 2011, on CD-ROM, Latin American Section (LAS) / American Nuclear Society (ANS)
ISBN 978-85-63688-00-2

IMPACT OF SPHERICAL INCLUSION MEAN CHORD LENGTH AND RADIUS DISTRIBUTION ON THREE-DIMENSIONAL BINARY STOCHASTIC MEDIUM PARTICLE TRANSPORT

Patrick S. Brantley* **and Jenny N. Martos†**
Lawrence Livermore National Laboratory
P.O. Box 808
Livermore, CA 94551 USA
brantley1@llnl.gov

ABSTRACT

We describe a parallel benchmark procedure and numerical results for a three-dimensional binary stochastic medium particle transport benchmark problem. The binary stochastic medium is composed of optically thick spherical inclusions distributed in an optically thin background matrix material. We investigate three sphere mean chord lengths, three distributions for the sphere radii (constant, uniform, and exponential), and six sphere volume fractions ranging from 0.05 to 0.3. For each sampled independent material realization, we solve the associated transport problem using the Mercury Monte Carlo particle transport code. We compare the ensemble-averaged benchmark fiducial tallies of reflection from and transmission through the spatial domain as well as absorption in the spherical inclusion and background matrix materials. For the parameter values investigated, we find a significant dependence of the ensemble-averaged fiducial tallies on both sphere mean chord length and sphere volume fraction, with the most dramatic variation occurring for the transmission through the spatial domain. We find a weaker dependence of most benchmark tally quantities on the distribution describing the sphere radii, provided the sphere mean chord length used is the same in the different distributions. The exponential distribution produces larger differences from the constant distribution than the uniform distribution produces. The transmission through the spatial domain does exhibit a significant variation when an exponential radius distribution is used.

Key Words: binary stochastic medium, Monte Carlo, particle transport

1. INTRODUCTION

A stochastic medium is one in which the material properties at a given point in space are only known statistically [1]. Particle transport through stochastic media is encountered in various applications. High temperature gas-cooled reactors contain microsphere fuel kernels of a constant size stochastically distributed in a graphite matrix within a spherical fuel pebble or a cylindrical fuel compact [2, 3]. Neutron transport in boiling water reactors involves transport through a stochastic medium composed of liquid water and water vapor [1], in which case the water vapor bubbles can be modeled as spheres of different sizes as a result of bubble coalescence

*Corresponding author
†Current address: Department of Nuclear Engineering, University of California, Berkeley, 4155 Etcheverry Hall, Berkeley, CA 94720 USA

and breakup [4]. Inertial confinement fusion targets may develop hydrodynamic instabilities at material interfaces resulting in particle transport through a turbulent mixture [1, 5] involving materials of varying size and shape [6, 7]. The work in this paper is aimed at turbulent mixture problems and investigates the impact of varying inclusion size and different size distributions on particle transport through a binary stochastic medium.

The development of algorithms to simulate particle transport through binary stochastic mixtures has received significant research attention in the last two decades [1, 8]. Much of the research has focused on the development and analysis of approximate models for the solution of such particle transport problems. The most common approach to solving particle transport problems involving binary stochastic media is to use the atomic mix approximation [1] in which the transport problem is solved using ensemble-averaged material properties. The atomic mix approximation is appealing because of its simplicity and computational efficiency but may not be accurate enough depending on the details of the stochastic material properties. The most ubiquitous approximate deterministic model developed specifically for solving binary stochastic media transport problems is often referred to as the Levermore-Pomraning model or the Standard Model [1, 8]. Zimmerman [9] and Zimmerman and Adams [10] first proposed Monte Carlo algorithms for solving binary stochastic medium transport problems. They proposed a base Monte Carlo algorithm that is equivalent to the Levermore-Pomraning equations and another Monte Carlo algorithm that possesses increased accuracy as a result of improved local material realization modeling.

The accuracy of the Levermore-Pomraning deterministic model and the Zimmerman-Adams Monte Carlo models has previously been examined in one-dimensional planar geometry using a suite of benchmark problems involving a non-stochastic isotropic angular flux incident on one boundary of a binary stochastic medium [10, 11]. The benchmark results were generated by sampling independent material realizations, solving using a discrete ordinates algorithm the transport problem for each independent realization, and ensemble averaging the results. Recent work has extended the benchmark results to include interior source problems [12, 13].

Two-dimensional [14] and three-dimensional [3, 15–17] binary stochastic medium benchmark results have previously been generated for use in assessing the accuracy of Monte Carlo particle transport algorithms for binary stochastic media. The binary stochastic medium in these benchmark simulations consisted of spherical inclusions in a background matrix material. These benchmark results were obtained by sampling independent material realizations, solving using a Monte Carlo algorithm the transport problem for each independent realization, and ensemble averaging the results. In these examples, the radii of the spherical inclusions in the background matrix were assumed to be described by a constant distribution, i.e. the inclusions were of a single constant radius. This assumption is appropriate for the modeling of pebble bed reactors, for example, but may not be appropriate for the generation of benchmark results aimed at assessing the accuracy of algorithms for modeling particle transport through turbulent media. Two-dimensional binary stochastic medium benchmark results [6] have been generated for the case of material realizations with inclusions of random size and shape produced by the intersection of lines with lengths distributed according to Markovian statistics.

Olson [18] has generated two- and three-dimensional binary stochastic medium benchmark results for problems in which spherical inclusions have different constant radii as well as for the case in which the radius of the inclusions is described by an exponential distribution. The

work in that paper is aimed at photon transport problems in which the radiation field is coupled to the matter through a material energy balance equation, and the primary focus is on two-dimensional benchmark results. The three-dimensional benchmark results presented in the paper were obtained using a single material realization, did not include the effects of scattering for radiation-only problems, and used a low-order $P_{1/3}$ angular approximation to solve the transport problem with spatial resolution restricted by serial computing simulation time limitations. Because the benchmark results were obtained using a deterministic method, the geometry of the spherical inclusions was not modeled exactly.

In this paper, we focus on linear particle transport problems in a three-dimensional binary stochastic medium. We investigate the effect of varying inclusion sphere radius on the transport of particles through the medium. In particular, we investigate spherical inclusions whose radii are described by a constant, a uniform, and an exponential distribution. For the case of a constant distribution, we investigate the effects on the particle transport solution of differing radii of inclusions. The cases with spherical inclusions whose radii are distributed according to a uniform and an exponential distribution help to further assess the effects of differing radii in a single realization. For the benchmark transport problem investigated, the work in this paper investigates the questions of how the ensemble-averaged benchmark tallies vary as a function of 1) the spherical inclusion mean chord length (radius), 2) the spherical inclusion volume fraction, and 3) the distribution describing the spherical radii. The material parameters we use in this benchmark study are variations of parameters originally used by Adams et al. [11] in the generation of one-dimensional benchmark transport solutions and provide a connection to our recent related work [13]. We generate benchmark results by sampling independent material realizations, solving the transport problem for each independent realization using the Mercury Monte Carlo particle transport code [19], and ensemble averaging the tally results. Because we solve the transport problems using Monte Carlo particle transport, the geometry is modeled exactly and the solution of the transport problem involves no angular discretization or expansion truncation. In addition, we are able to simulate a large number of independent material realizations in a reasonable time using a parallel algorithm.

The work described in this paper improves the understanding of the impact of varying spherical inclusion radius and different radius distributions on particle transport through a binary stochastic medium. This understanding may prove beneficial for applications involving particle transport through turbulent media composed of inclusions of varying sizes. In addition, the benchmark results produced in this work will be useful in assessing the accuracy of multidimensional Monte Carlo particle transport algorithms aimed at solving these types of problems.

The remainder of this paper is organized as follows. We describe the benchmark transport problem along with the numerical procedures used to generate the benchmark solutions in Section 2. We examine the ensemble-averaged tally results obtained with the different sphere mean chord lengths and sphere radius distributions in Section 3. We give general conclusions and suggestions for future work in Section 4.

2. BENCHMARK TRANSPORT PROBLEM SUITE

In this section, we first describe the binary stochastic medium benchmark transport problem we investigate in this paper. We then describe the parallel procedure used to generate the

benchmark solutions.

We consider the following time-independent monoenergetic particle transport problem with isotropic scattering in a three-dimensional cubic spatial domain D defined by $0 \leq x, y, z \leq L$ with outer boundary ∂D:

$$\underline{\Omega} \cdot \underline{\nabla} \psi \left(\underline{x}, \underline{\Omega} \right) + \sigma_t \left(\underline{x} \right) \psi \left(\underline{x}, \underline{\Omega} \right) = \frac{\sigma_s \left(\underline{x} \right)}{4\pi} \int_{4\pi} \psi \left(\underline{x}, \underline{\Omega}' \right) d^2\Omega' \quad . \tag{1}$$

Here we have used standard neutronics notation [20]: ψ is the angular flux of particles [#/cm^2-s-steradian] at a position $\underline{x} = (x, y, z)$ traveling in direction $\underline{\Omega}$; $\sigma_t \left(\underline{x} \right)$ is the macroscopic total cross section [cm^{-1}] at position $\underline{x}$; and $\sigma_s \left(\underline{x} \right)$ is the macroscopic scattering cross section [cm^{-1}] at position $\underline{x}$. An isotropic angular flux with unity incoming current is incident on the left edge of the domain at $x = 0$:

$$\psi \left(x = 0, y, z, \underline{\Omega} \right) = \frac{1}{2\pi} \quad , \quad 0 \leq y, z \leq L \quad , \quad \underline{\Omega} \cdot \underline{n} < 0 \quad , \tag{2}$$

where $\underline{n}$ is the unit outer normal to ∂D at a position $\underline{x}$ on the boundary. A vacuum boundary condition is imposed on the right edge of the domain at $x = L$:

$$\psi \left(x = L, y, z, \underline{\Omega} \right) = 0 \quad , \quad 0 \leq y, z \leq L \quad , \quad \underline{\Omega} \cdot \underline{n} < 0 \quad . \tag{3}$$

The boundaries on all other transverse edges of the cubic domain are reflecting. The transport problem is depicted schematically in Fig. 1. We assume that the binary stochastic medium is composed of optically thick spherical inclusions with uniform material properties distributed in an optically thin background matrix material also with uniform material properties. The benchmark ensemble-averaged fiducial quantities of interest are the reflection and transmission rates as well as the absorption rates in the sphere and background matrix materials.

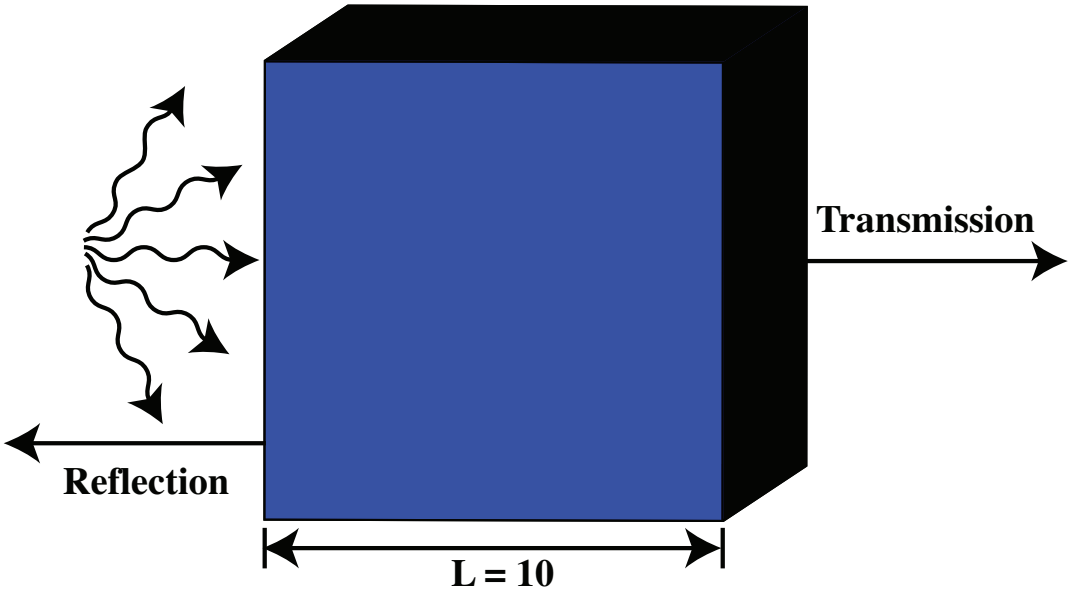

Figure 1: Transport problem configuration.

We investigate a suite of binary stochastic medium benchmark problems characterized by the material parameters given in Table I. Here material zero is an optically thin background matrix material, material one is an optically thick spherical inclusion material, and Λ_i is the mean chord length for material i. Both materials are assumed to have a scattering ratio of $c = \sigma_s/\sigma_t = 0.9$. These material parameters are variations of parameters originally used by Adams et al. [11] in the generation of one-dimensional benchmark transport solutions and provide a connection with recent related work [13]. The different case numbers in our benchmark suite represent variations of the spherical inclusion radii as defined by the mean chord length through the sphere. The mean chord length for any non-reentrant body is given by $\Lambda = 4V/A$, where V is the volume of the body and A is the surface area of the body. For a sphere of radius R, $\Lambda_{sphere} = 4R/3$. Different distributions of sphere radii characterized by a mean radius R will have different mean chord length values, as described below. For each sphere mean chord length case (1, 2, and 3), six different sphere volume fractions f_1 (0.05, 0.10, 0.15, 0.20, 0.25, and 0.30) are considered, where the sphere volume fraction f_1 is defined as the total volume of all spherical inclusions divided by the volume of the problem domain. If the sphere volume fraction f_1 and the sphere mean chord length Λ_1 are known, the mean chord length in the background matrix material can be computed as $\Lambda_0 = (1/f_1 - 1)\,\Lambda_1$ [1, 21] for an infinite medium (ignoring boundary effects). Consistent with previous one-dimensional work [11, 13], we assume a domain size of $L = 10$.

Table I: Material parameters for benchmark transport problems

Case	σ_t^0	Λ_0^*	$\sigma_t^0\Lambda_0$	σ_t^1	Λ_1	$\sigma_t^1\Lambda_1$	c
1		99/40	0.25		11/40	2.5	
2	10/99	99/20	0.5	100/11	11/20	5.0	0.9
3		99/10	1.0		11/10	10.0	

* For 10% sphere volume fraction

Adams et al. [11] investigated in one spatial dimension a significantly broader range of material parameters. However, this broader range of parameters results in a significant proliferation of test cases to be simulated and an ensuing difficulty in productively analyzing the resulting large amount of data. As a result, we have chosen to restrict our benchmark suite to a single set of macroscopic total cross sections as given in Table I, with both the matrix and sphere materials having a scattering ratio of $c = \sigma_s/\sigma_t = 0.9$.

We generated the benchmark solutions using an extension of the parallel methodology previously described in Ref. [13]. The benchmark procedure generally consists of using a Python driver script to 1) sample an independent material realization and write the spherical inclusion locations and radii to a file, 2) solve the transport problem using the Mercury Monte Carlo particle transport code [19] for the sampled realization and tally the leakage and absorption rates for that realization, and 3) average the tally results for all realizations to obtain ensemble-averaged values. One instance of an independent material realization is generated using a random sequential addition (RSA) technique [22] by 1) sampling the radii of the spheres from the appropriate distribution until the desired sphere volume fraction is reached, 2) uniformly sampling the (x, y, z) points for sphere locations, and 3) rejecting spheres overlapping previously-sampled spheres or the problem boundary. We have implemented a C++ code that can use either a simple RSA

method or a "fast RSA" method proposed by Brown [23] when the number of spheres to be sampled is large.

We investigate three sphere radius distributions in this paper: a constant distribution, a uniform distribution, and an exponential distribution. These distributions were previously used by Olson et al. [21] in the investigation of background chord length distributions in binary stochastic media. The radius probability distribution function $p(r)$ for each of the distributions along with the relationship between the sphere mean chord length Λ_1 and the sphere mean radius R [21] are given by

- Constant radius distribution: $p(r) = \delta(r - R)$, $R = \frac{3}{4}\Lambda_1$;
- Uniform radius distribution: $p(r) = \frac{1}{2R}$ for $0 \leq r \leq 2R$, $R = \frac{1}{2}\Lambda_1$;
- Exponential radius distribution: $p(r) = \frac{1}{R}\exp\left(-\frac{r}{R}\right)$ for $0 \leq r \leq \frac{L}{6}$, $R = \frac{1}{4}\Lambda_1$.

During the sampling of the material realizations, the appropriate number of spheres are sampled to produce the desired sphere volume fraction. For the constant radius distribution, we sampled the number of spheres required to equal or exceed the desired sphere volume fraction. For the uniform and exponential radius distributions, the last sampled sphere radius was reduced to exactly produce the desired sphere volume fraction. For the exponential radius distribution, we heuristically limited the maximum sampled sphere radius to be 1/6 of the domain edge length L to avoid problems placing multiple large spheres in the problem domain. Because only sphere locations are rejected and resampled (not the sphere radii) during the generation of a realization, no skew towards smaller sphere radii is introduced for the uniform and exponential sphere radius distributions.

Because no spheres are allowed to overlap the vacuum and reflecting boundaries of the problem domain, the distribution of spheres near these boundaries will be different than in the interior of the spatial domain [21]. The extent of this boundary layer region in a given material realization depends on the maximum sphere radius in the realization. Additional work is required to quantify the impact of this effect on our benchmark results. The boundary layer effect near the transverse reflecting boundaries could be reduced (at the cost of additional computing expense) by using a significantly larger width in those dimensions.

Given a single material realization of the binary stochastic medium, the transport problem described by Eqs. (1)–(3) is solved for that realization using the Mercury Monte Carlo particle transport code [19]. For each material realization, the tally quantities of interest are the reflection and transmission rates as well as the absorption rates in the sphere and background matrix materials. This procedure is repeated a large number M of times and the results averaged to obtain ensemble-averaged values. The ensemble-averaged reflection rate at $x = 0$, $\langle J_{reflection} \rangle$, is given by

$$\langle J_{reflection} \rangle = \frac{1}{M} \sum_{m=1}^{M} \int_0^L \int_0^L \int_{\underline{\Omega}\cdot\underline{n}>0} \underline{\Omega} \cdot \underline{n} \psi_m (x = 0, y, z, \underline{\Omega}) \, d\underline{\Omega} dy dz \quad , \tag{4}$$

where $\psi_m(x, y, z, \underline{\Omega})$ is the angular flux computed for realization m and $\underline{n}$ is the unit outer normal to ∂D at a position $\underline{x} = (0, y, z)$ on the boundary. Similarly, the ensemble-averaged

transmission rate at $x = L$, $\langle J_{transmission} \rangle$, is given by

$$\langle J_{transmission} \rangle = \frac{1}{M} \sum_{m=1}^{M} \int_0^L \int_0^L \int_{\underline{\Omega} \cdot \underline{n} > 0} \underline{\Omega} \cdot \underline{n} \psi_m \left(x = L, y, z, \underline{\Omega} \right) d\underline{\Omega} dy dz \quad . \tag{5}$$

The reflection and transmission rates were tallied in Mercury for each material realization using an analog estimator. The ensemble-averaged absorption rate in material i, $\langle A_i \rangle$, $i = 0, 1$, is given by

$$\langle A_i \rangle = \frac{1}{M} \sum_{m=1}^{M} \int_D \chi_{i,m} \left(\underline{x} \right) \sigma_t^i \left(1 - c \right) \int_{4\pi} \psi_m \left(\underline{x}, \underline{\Omega} \right) d\underline{\Omega} d\underline{x} \quad , \tag{6}$$

where c is the scattering ratio and $\chi_{i,m} \left(\underline{x} \right)$ is a characteristic function that is unity if material i is present at location $\underline{x}$ in material realization m and is zero otherwise. The material absorption rates were tallied in Mercury for each material realization using a pathlength estimator.

In addition to the ensemble-averaged tally values described above, we also compute the standard deviation in the realization tallies about the ensemble-averaged mean value. This standard deviation gives an indication of the spread of the independent material realization tally values about the ensemble-averaged mean value. For a generic tally Q, the standard deviation, σ_Q, is given by

$$\sigma_Q = \sqrt{\langle Q^2 \rangle - \langle Q \rangle^2} \quad , \tag{7}$$

where $\langle Q \rangle$ and $\langle Q^2 \rangle$ are the ensemble-averaged mean and mean squared tally values, respectively. An estimate of the standard deviation of the ensemble-averaged mean tally $\langle Q \rangle$, $\sigma_{\langle Q \rangle}$, is given by

$$\sigma_{\langle Q \rangle} = \frac{\sigma_Q}{\sqrt{M}} \quad . \tag{8}$$

This estimated standard deviation provides an estimate of the uncertainty of the ensemble-averaged mean tally value about the true mean value. Because we used a Monte Carlo algorithm to solve the transport problem associated with the independent material realization, Eqs. (7) and (8) should include a term accounting for the stochastic nature of the Monte Carlo solution. The Mercury Monte Carlo particle transport code does not currently provide statistical uncertainty estimates for the user-defined tallies used to obtain the results in this paper. As a result, our statistical uncertainty estimates must currently be viewed as lower bounds. In the discussion of our numerical results, we quote the standard deviation as a relative value defined as $\sigma_{\langle Q \rangle} / \langle Q \rangle$.

We use a parallel algorithm to generate the benchmark results in order to increase the computational efficiency of the benchmark procedure. The Python driver script uses the pyMPI [24] Python extension to parallelize using the MPI message passing interface [25] the simulation of the independent material realizations. The total number of realizations to be simulated are divided among the allocated processors. Each Mercury simulation can be run using one processor or using multiple processors with particle parallelism, where the number of processors is designated by the user. For a given total number of available processors P, one can choose to simultaneously run P independent Mercury simulations on one processor each or P/K independent Mercury simulations on $K - 1$ processors each (the other processor is used to run the Python driver script and the C++ code used to sample the material realizations.) This parallelization algorithm is very efficient, as each independent material realization can be simulated with no parallel communication with other processes required until all of its computational work is completed. Care must be exercised to ensure that independent random number streams are utilized on each MPI process.

3. NUMERICAL RESULTS

In this section, we present the numerical results for the binary stochastic medium benchmark simulations performed. The benchmark simulations were performed on the Zeus machine at Lawrence Livermore National Laboratory, a Linux cluster with eight Intel 2.4 GHz CPUs per compute node. Each benchmark simulation used 50 nodes (400 processors), with each Mercury simulation using seven processors of the node to simulate the particle transport and one processor dedicated to running the Python driver script and the material realization sampling code.

The benchmark results were generated using $M = 100$ independent material realizations for each sphere mean chord length case, for each sphere volume fraction value, and for each sphere radius distribution. As a result, the benchmark results described in this paper required a total of 5,400 three-dimensional Monte Carlo particle transport simulations. Each Monte Carlo simulation for an independent material realization used 2×10^6 particle histories. This number of Monte Carlo particles was chosen such that each benchmark set of $M = 100$ independent material realizations would complete in the maximum batch job limit (sixteen hours) on the Zeus machine. With this number of particles, the standard deviation of the ensemble-averaged mean for each tally was computed to be less than 2% for all cases. (We generated independent benchmark suite numerical results from 5,400 simulations using a different random number stream, and the ensemble-averaged tally values agreed with the original suite to within 2.2% in all cases.) The compute time required for each benchmark set of $M = 100$ realizations varied from less than one minute to 675 minutes. The set with the smallest mean chord length (case 1) and largest sphere volume fraction value (0.3) were the most expensive to compute as a result of the larger number of spheres and hence Monte Carlo cells in the problem. The exponential sphere radius distribution results were the most expensive to obtain.

3.1 Constant Sphere Radius Distribution Results

In this section, we examine the benchmark results for cases in which the spheres have a constant radius for a given set of material realizations. The different sphere mean chord length cases have different constant sphere radii, so our results demonstrate the effects of differing sphere radii on the ensemble-averaged reflection, transmission, sphere absorption, and matrix absorption rates. These benchmark results also demonstrate the impact of sphere volume fraction on the ensemble-average tally values. The ensemble-averaged tally results are plotted in Fig. 2.

The reflection rate for the different sphere mean chord length cases and sphere volume fractions are plotted (with a suppressed zero) in Fig. 2(a). For a given sphere volume fraction, the reflection rate decreases with increasing sphere radius (i.e. the case 3 reflection rate is lower than the case 1 reflection rate). For a given sphere mean chord length case, the reflection rate is relatively constant but exhibits a non-monotonic behavior with increasing sphere volume fraction and is highest at the largest sphere volume fraction.

The transmission rate for the different sphere mean chord length cases and sphere volume fraction values are plotted on a log scale in Fig. 2(b). Significant differences can be observed in the transmission rates for the different sphere mean chord length cases and different sphere volume fractions. For a given sphere volume fraction, the transmission rate increases with increasing sphere radius (i.e. the case 3 transmission rate is higher than the case 1 rate). The differences in

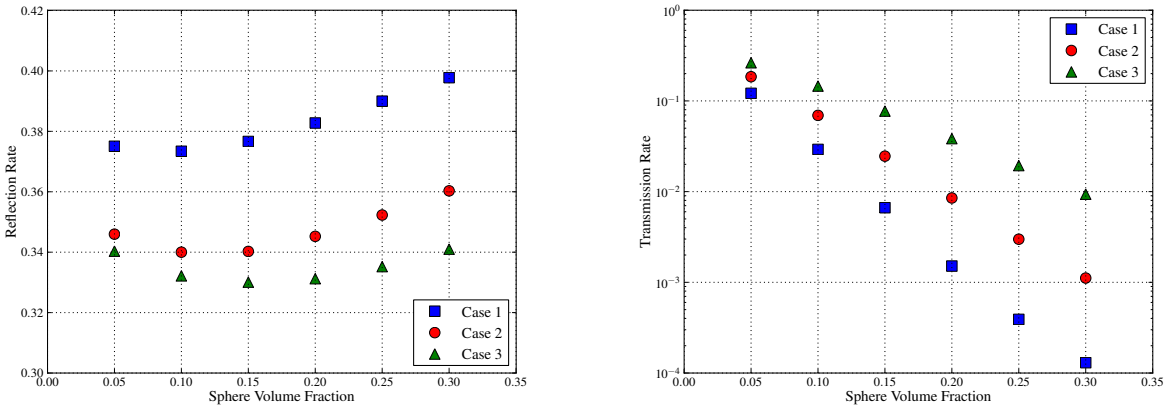

(a) Reflection rate

(b) Transmission rate

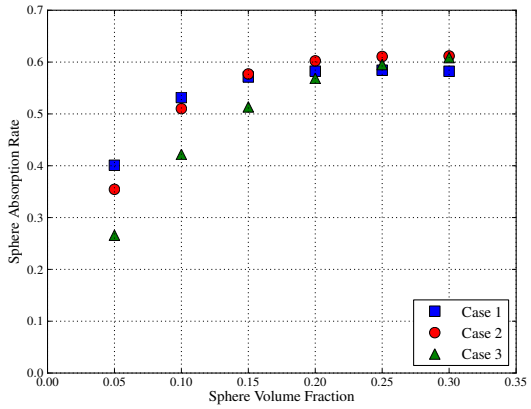

(c) Sphere absorption rate

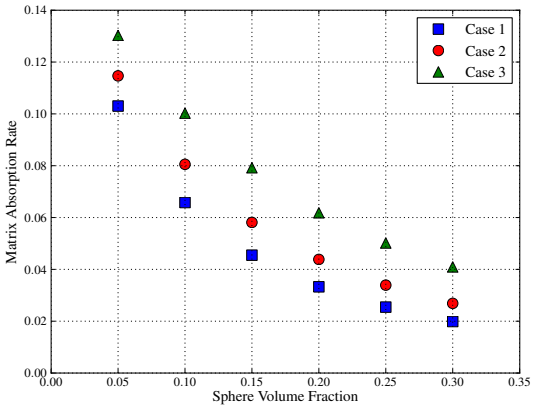

(d) Matrix absorption rate

Figure 2: Constant sphere radius distribution ensemble average tally results.

transmission rate between the sphere mean chord length cases increase with increasing sphere volume fraction. These effects can be explained by the presence of larger streaming paths for cases with larger sphere radii. For a given sphere mean chord length case, the transmission rate decreases significantly with increasing sphere volume fraction as a result of increased absorption in the spherical inclusions.

The absorption rate in the spherical inclusions for the different sphere mean chord length cases and sphere volume fractions are plotted in Fig. 2(c). For all sphere mean chord length cases, the absorption rate in the spherical inclusions monotonically increases with increasing sphere volume fraction. At lower sphere volume fractions, significant differences in the absorption rate are observed between the different sphere mean chord length cases. The absorption rate in the spherical inclusions limits to approximately 0.6 for all cases at higher sphere volume fractions.

The absorption rate in the background matrix for the different sphere mean chord length cases and sphere volume fractions are plotted in Fig. 2(d). For all cases, the absorption rate in the background matrix monotonically decreases as the sphere volume fraction increases. For a given

sphere volume fraction, the background matrix absorption rate decreases with decreasing sphere radius (i.e. the case 3 rate is higher than the case 1 rate).

Overall, we find significant variations in the ensemble-averaged tally results for the different sphere mean chord lengths and sphere volume fractions.

3.2 Uniform and Exponential Sphere Radius Distribution Results

In this section, we present benchmark results for cases in which the radii of the spheres are given by the uniform and exponential distributions described in Section 2. The mean radius used in each distribution is obtained from the sphere mean chord length in Table I using the relationship in Section 2. The mean chord lengths in the spheres used for the different cases in this section are the same as those used in the constant radius results of Section 3.1. Compared to the constant radius distribution results, these sets of benchmark results demonstrate the effects of different sphere radii within individual material realizations. To facilitate these comparisons, we plot in Figs. 3 and 4 the ratio of the ensemble-averaged tally obtained using the given radius distribution to the value of that tally obtained using the constant radius distribution.

As a general result, we first observe that the ensemble-averaged tallies from the exponential radius distribution exhibit larger departures from the constant radius distribution results than the uniform radius distribution.

The reflection rate for both the uniform and exponential radius distributions agrees with the constant radius distribution result to within approximately 3%, with the largest differences occurring for the exponential distribution and cases 2 and 3 (i.e. the larger sphere radius cases). The tally ratios are greater than unity in nearly all cases, demonstrating that the reflection rate obtained with the uniform and exponential sphere radius distributions is higher than for the constant distribution. Given the approximately 2% statistical uncertainty in our results, we conclude that the reflection rate is insensitive to the distribution describing the spherical inclusion radius.

The transmission rate exhibits the largest departures from the constant radius distribution results, with differences up to approximately 10% for the uniform radius distribution and up to approximately 40% for the exponential radius distribution. We note that the transmission rate obtained using the uniform and exponential radius distributions is higher than for the constant radius distribution for all sphere mean chord lengths and sphere volume fractions. Because the volume of a sphere scales as the cube of the radius, spheres that are larger than the mean account for a disproportionately larger part of the total sphere volume fraction. The presence of these larger spheres in a realization introduces additional open streaming paths for particles, resulting in a higher transmission rate. The transmission rate ratios are typically higher for larger sphere volume fractions. We conclude that the transmission rate is sensitive to the distribution describing the spherical inclusion radius, with the exponential radius distribution particularly producing significantly different transmission rates than the constant distribution.

The sphere absorption rate computed using the uniform and exponential radius distributions is in all instances lower than for the constant radius distribution. The largest differences occur at the lower sphere volume fractions. The uniform distribution produces sphere absorption rates lower than the constant distribution by approximately 3% at the lowest sphere volume fractions, while

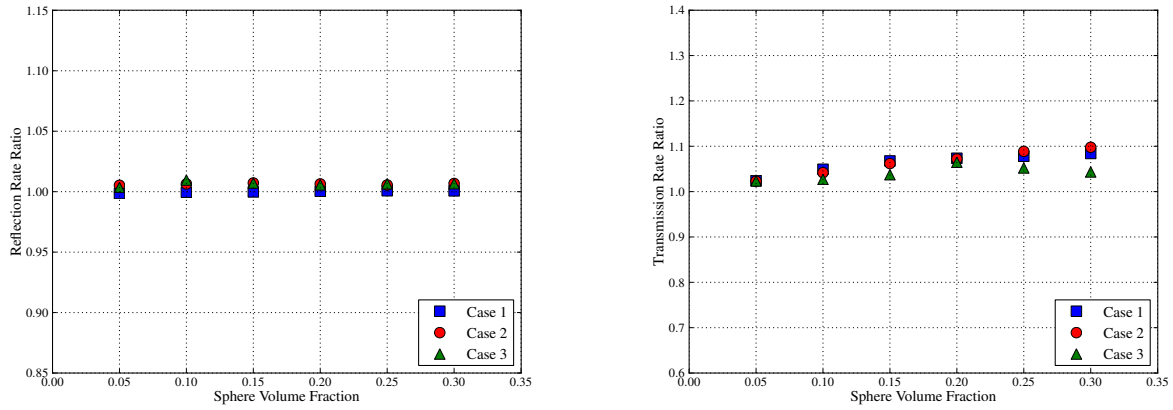

(a) Reflection rate ratio

(b) Transmission rate ratio

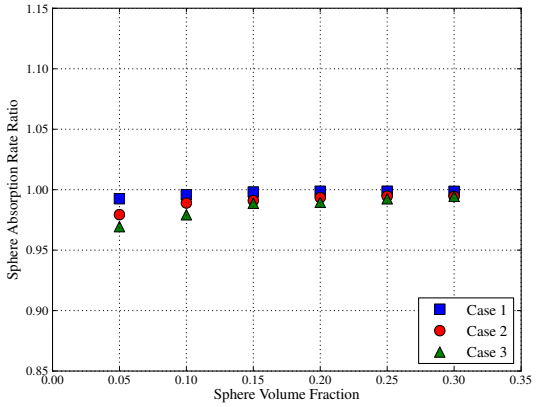

(c) Sphere absorption rate ratio

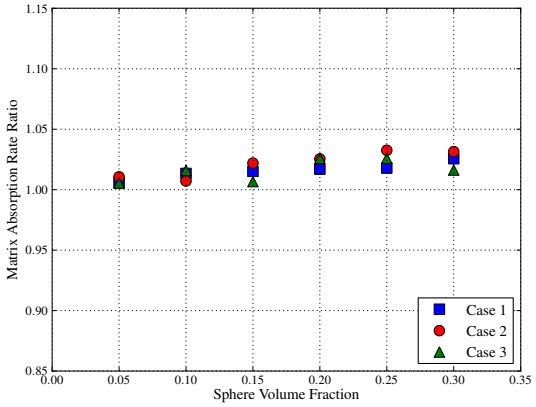

(d) Matrix absorption rate ratio

Figure 3: Uniform sphere radius distribution ensemble average tally to constant distribution tally ratios.

the exponential distribution produces differences of approximately 7%. The sphere absorption rates agree to within approximately 1-2% at the higher sphere volume fractions. Therefore, the sphere absorption rate is largely independent of the sphere radius distribution at larger sphere volume fractions. We conclude that the sphere absorption rate is weakly sensitive to the distribution describing the spherical inclusion radius.

The matrix absorption rate computed using the uniform and exponential radius distributions is in all instances higher than for the constant radius distribution. The differences are generally largest at the higher values of the sphere volume fraction, with the uniform radius distribution producing values up to approximately 3% larger and the exponential radius distribution up to approximately 10% larger. We conclude that the matrix absorption rate is weakly sensitive to the distribution describing the spherical inclusion radius.

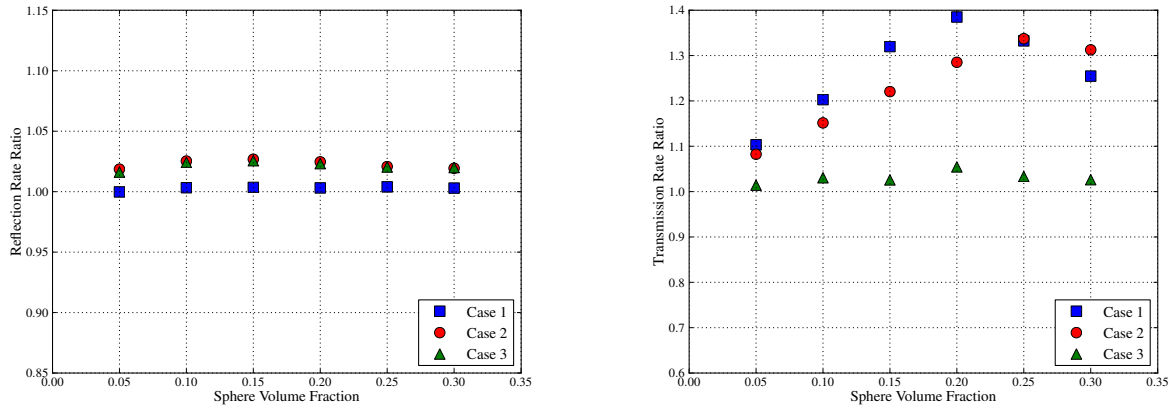

(a) Reflection rate ratio

(b) Transmission rate ratio

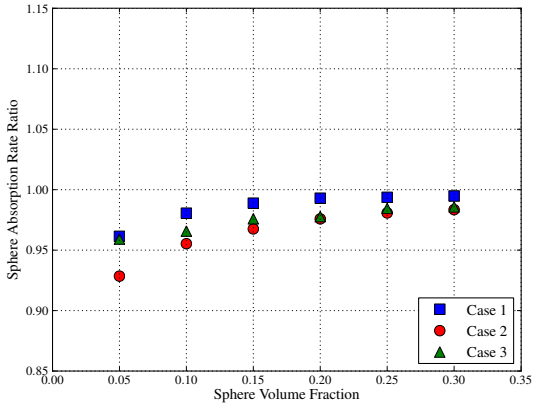

(c) Sphere absorption rate ratio

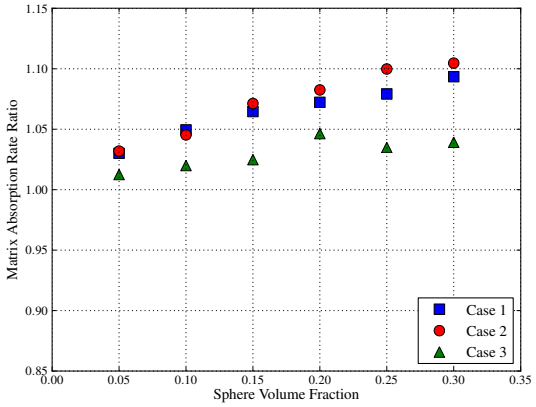

(d) Matrix absorption rate ratio

Figure 4: Exponential sphere radius distribution ensemble average tally to constant distribution tally ratios.

3.3 Standard Deviation Results

In this section, we briefly summarize the statistical uncertainty estimates for our benchmark numerical results. The estimated standard deviation of the ensemble-averaged mean reflection rate, transmission rate, and absorption rates in the sphere and background matrix materials are less than 2% for all cases examined. (As noted above, we generated independent benchmark suite numerical results from 5,400 simulations using a different random number stream. The ensemble-averaged tally values from the duplicate suite agreed with the original suite to within 2.2% in all cases, with most differences less than 1%.) The reflection rate standard deviation values are generally the smallest while the transmission rate standard deviation values are generally the largest. The standard deviation values increase with increasing mean sphere radius. The constant and uniform sphere radius distributions produce similar standard deviations, while the exponential distribution produces notably larger standard deviations.

Because we simulated $M = 100$ independent material realizations, the standard deviations of the material realization tallies about the mean are a factor of $\sqrt{M} = 10$ larger than the estimated standard deviation of the tally mean about the true mean. As a result, the largest estimated standard deviations of the material realizations approach 20% for the transmission rate tally with the exponential radius distribution.

4. CONCLUSIONS

We described a parallel benchmark procedure and numerical results for a three-dimensional binary stochastic medium particle transport benchmark problem. The binary stochastic medium is composed of optically thick spherical inclusions distributed in an optically thin background matrix material. We investigated three sphere mean chord lengths, three distributions for the sphere radii (constant, uniform, and exponential), and six sphere volume fractions ranging from 0.05 to 0.3. We compared the ensemble-averaged benchmark fiducial tallies of reflection from and transmission through the spatial domain as well as absorption in the spherical inclusion and background matrix materials. For the parameter values investigated, our benchmark results exhibit a significant dependence of the ensemble-averaged fiducial tallies on both sphere mean chord length and sphere volume fraction, with the most dramatic variation occurring for the transmission through the spatial domain. Our benchmark results exhibit a weaker dependence of most benchmark tally quantities on the distribution describing the sphere radii, provided the sphere mean chord length used is the same in the different distributions. The exponential distribution produces larger differences from the constant distribution than the uniform distribution produces. The transmission through the spatial domain does exhibit a significant variation when an exponential radius distribution is used.

The findings of our benchmark study are somewhat in contrast to those of Olson [18], who found that different sphere radii gave similar results for a given sphere volume fraction. However, Olson used a smaller spatial domain size of $L = 1$ and investigated spherical inclusions with mean chord lengths at least an order of magnitude smaller than the smallest mean chord length in our study. Future work covering a broader range of domain sizes and material parameters will be required to resolve these discrepancies.

In future work, we plan to investigate additional mean chord length cases and different material parameters. In addition, we plan to investigate additional inclusions shapes (e.g. ellipsoids) to evaluate the impact of non-spherical inclusion shapes. Finally, the ultimate goal of this work is to generate benchmark results to assess the accuracy of multi-dimensional Monte Carlo particle transport algorithms for stochastic medium benchmark problems. We plan to report on these comparisons in the future.

ACKNOWLEDGEMENTS

This work performed under the auspices of the U.S. Department of Energy by Lawrence Livermore National Laboratory under Contract DE-AC52-07NA27344. The work of the second author was performed under appointment to the LLNL High Energy Density Summer Student Program. The authors would like to acknowledge helpful conversations with Matt O'Brien and Brian Yang.

REFERENCES

1. G. C. Pomraning. *Linear Kinetic Theory and Particle Transport in Stochastic Mixtures.* World Scientific Publishing Co. Pte. Ltd., River Edge, New Jersey USA (1991).

2. I. Murata, T. Mori, M. Nakagawa. Continuous Energy Monte Carlo Calculations of Randomly Distributed Spherical Fuels in High-Temperature Gas-Cooled Reactors Based on a Statistical Geometry Model. *Nucl. Sci. Engr.*, **123**, pp. 96-109 (1996).

3. W. Ji, W. R. Martin. Monte Carlo Simulation of VHTR Particle Fuel with Chord Length Sampling. *Joint International Topical Meeting on Mathematics & Computation and Supercomputing in Nuclear Applications (M&C + SNA 2007)*, Monterey, CA, April 15-19, 2007, on CD-ROM, American Nuclear Society, La Grange Park, IL (2007).

4. Q. Wu, S. Kim, M. Ishii, S. Beus. One-Group Interfacial Area Transport in Vertical Bubbly Flow. *Int. J. Heat Mass Transfer*, **41**, pp. 1103-1112 (1998).

5. C. D. Levermore, G. B. Zimmerman. Modeling Charged Particle Loss in a Fuel/Shell Mixture. *J. Math. Phys.*, **34**, pp. 4725-4729 (1993).

6. O. Haran, D. Shvarts, R. Thieberger. Transport in Two-Dimensional Scattering Stochastic Media: Simulations and Models. *Phys. Rev. E*, **61**, pp. 6183-6189 (2000).

7. P. Keiter, M. Gunderson, J. Foster, P. Rosen, A. Comley, M. Taylor, T. Perry. Radiation Transport in Inhomogeneous Media. *Phys. Plasmas*, **15** (2008).

8. C. D. Levermore, G. C. Pomraning, D. L. Sanzo, J. Wong. Linear Transport Theory in a Random Medium. *J. Math. Phys.*, **27**, pp. 2526-2536 (1986).

9. G. B. Zimmerman. Recent Developments in Monte Carlo Techniques. Lawrence Livermore National Laboratory Report UCRL-JC-105616 (1990).

10. G. B. Zimmerman, M. L. Adams. Algorithms for Monte-Carlo Particle Transport in Binary Statistical Mixtures. *Trans. Am. Nucl. Soc.*, San Francisco, CA, November 10-14, 1991, Vol. 64, p. 287 (1991).

11. M. L. Adams, E. W. Larsen, G. C. Pomraning. Benchmark Results for Particle Transport in a Binary Markov Statistical Medium. *J. Quant. Spectrosc. Radiat. Transfer*, **42**, pp. 253-266 (1989).

12. P. S. Brantley, T. S. Palmer. Levermore-Pomraning Model Results for an Interior Source Binary Stochastic Medium Benchmark Problem. *Proceedings of the International Conference on Mathematics, Computational Methods & Reactor Physics (M&C 2009)*, Saratoga Springs, New York, May 3-7, 2009, on CD-ROM, American Nuclear Society, La Grange Park, IL (2009).

13. P. S. Brantley. A Benchmark Comparison of Monte Carlo Particle Transport Algorithms for Binary Stochastic Mixtures. *J. Quant. Spectrosc. Radiat. Transfer*, **112**, pp. 599-618 (2011).

14. T. J. Donovan, Y. Danon. Application of Monte Carlo Chord-Length Sampling Algorithms to Transport Through a Two-Dimensional Binary Stochastic Mixture. *Nucl. Sci. Engr.*, **143**, pp. 226-239 (2003).

15. T. J. Donovan, Y. Danon. Implementation of Chord Length Sampling for Transport Through a Binary Stochastic Mixture. *Proceedings of the Nuclear Mathematical and Computational Sciences: A Century in Review, A Century Anew*, Gatlinburg, TN, April 6-11, 2003, on CD-ROM, American Nuclear Society, La Grange Park, IL (2003).

16. T. J. Donovan, Y. Danon. HTGR Unit Fuel Pebble k-infinity Results Using Chord Length Sampling. *Trans. Am. Nucl. Soc.*, New Orleans, LA, November 16-20, 2003, Vol. 89, pp. 37-39 (2003).

17. D. R. Reinert, E. A. Schneider, S. R. F. Biegalski, Investigation of Stochastic Radiation Transport Methods in Binary Random Heterogeneous Mixtures. *Nucl. Sci. Engr.*, **166**, pp. 167-174 (2010).

18. G. L. Olson. Gray Radiation Transport in Multi-Dimensional Stochastic Binary Media with Material Temperature Coupling. *J. Quant. Spectrosc. Radiat. Transfer*, **104**, pp. 86-98 (2007).

19. R. J. Procassini, P. S. Brantley, S. A. Dawson, G. M. Greenman, M. S. McKinley, M. J. O'Brien. Mercury User Guide: Version c.8. UCRL-TM-204296 (Revision 7), Lawrence Livermore National Laboratory Report (2010).

20. E. E. Lewis, W. F. Miller. *Computational Methods of Neutron Transport*. American Nuclear Society, La Grange Park, Illinois, USA (1993).

21. G. L. Olson, D. S. Miller, E. W. Larsen, J. E. Morel. Chord Length Distributions in Binary Stochastic Media in Two and Three Dimensions. *J. Quant. Spectrosc. Radiat. Transfer*, **101**, pp. 269-283 (2006).

22. B. Widom. Random Sequential Addition of Hard Spheres to a Volume. *J. Chem. Phys.*, **44**, pp. 3888-3894 (1966).

23. F. B. Brown. A Fast RSA Method for Fuel Particle Sphere Volume. *Trans. Am. Nucl. Soc.*, v. 94, pp. 571-573 (2006).

24. P. Miller. pyMPI - An Introduction to Parallel Python Using MPI. Lawrence Livermore National Laboratory Report UCRL-WEB-151052 (2002). See also http://pympi.sourceforge.net (2009).

25. W. Gropp, E. Lusk, A. Skjellum. *Using MPI: Portable Parallel Programming with the Message-Passing Interface*. The MIT Press, Cambridge, Massachusetts, USA (1999).